Neuroinformatics (2019) 17:295–306
https://doi.org/10.1007/s12021-018-9400-2

ORIGINAL ARTICLE

Rhesus Macaque Brain Atlas Regions Aligned to an MRI Template

Jeffrey M. Moirano[1] · Gleb Y. Bezgin[2,3,4,5] · Elizabeth O. Ahlers[1] · Rolf Kötter[3,4,5] · Alexander K. Converse[1]

Published online: 5 October 2018

Abstract

To aid in the analysis of rhesus macaque brain images, we aligned digitized anatomical regions from the widely used atlas of Paxinos et al. to a published magnetic resonance imaging (MRI) template based on a large number of subjects. Digitally labelled atlas images were aligned to the template in 2D and then in 3D. The resulting grey matter regions appear qualitatively to be well registered to the template. To quantitatively validate the procedure, MR brain images of 20 rhesus macaques were aligned to the template along with regions drawn by hand in striatal and cortical areas in each subject's MRI. There was good geometric overlap between the hand drawn regions and the template regions. Positron emission tomography (PET) images of the same subjects showing uptake of a dopamine D_2 receptor ligand were aligned to the template space, and good agreement was found between tracer binding measures calculated using the hand drawn and template regions. In conclusion, an anatomically defined set of rhesus macaque brain regions has been aligned to an MRI template and has been validated for analysis of PET imaging in a subset of striatal and cortical areas. The entire set of over 200 regions is publicly available at https://www.nitrc.org/.

Keywords Rhesus macaque · Brain · Atlas · Regions of interest · Positron emission tomography (PET) · Magnetic resonance imaging (MRI)

Rolf Kotter is deceased (Stephan et al. 2010). His coauthors are grateful for his contributions to this work.

Research Highlights
- Anatomical regions from the Paxinos atlas were aligned to a published MRI template
- ROIs were validated against hand drawn ROIs for PET image analysis
- The full set of aligned ROIs is available online.

Electronic supplementary material The online version of this article (https://doi.org/10.1007/s12021-018-9400-2) contains supplementary material, which is available to authorized users.

✉ Alexander K. Converse
alexander.converse@wisc.edu

[1] Waisman Center, University of Wisconsin-Madison, Madison, WI, USA

[2] Montreal Neurological Institute, McGill University, Montreal, QC H3A 2B4, Canada

[3] Department of Neuroinformatics, Donders Institute for Brain, Cognition and Behaviour, Radboud University Nijmegen, 6525 AJ Nijmegen, The Netherlands

[4] C.& O. Vogt Brain Research Institute, Heinrich Heine University, D-40225 Düsseldorf, Germany

[5] Institute of Anatomy II, Heinrich Heine University, D-40225 Düsseldorf, Germany

Introduction

In the analysis of neuroimaging data it is often necessary to define regions of interest (ROI) or to identify the location of voxels within the brain. This task can be made easier and also more reproducible by means of a labelled template image that is suitable as a registration target. Examples of such labelled templates are available for humans and rodents (Tzourio-Mazoyer et al. 2002; Rubins et al. 2003). In recent years, such templates have become available for macaques as well (Frey et al. 2011; Rohlfing et al. 2012; Van Essen et al. 2012; Shi et al. 2017; Ballanger et al. 2013). In the present work, we describe the alignment of the Paxinos et al. (2009) rhesus brain atlas to a rhesus MRI template based on a large number of subjects (McLaren et al. 2009). We developed this 3D digital brain atlas to aid in work with rhesus macaque positron emission tomography (PET) brain imaging (Converse et al. 2013; Converse et al. 2014; Christian et al. 2013; Wooten et al. 2013; Hillmer et al. 2014), and it has proven useful for diffusion tensor MRI work as well (Adluru et al. 2012; Zakszewski et al. 2014).

The rhesus macaque is the most commonly used non-human primate model of human brain anatomy and function (Paxinos et al. 2009). Advances in image resolution have facilitated brain research in macaques by PET (Tai et al. 2001).

Neuroimaging with PET and magnetic resonance imaging (MRI) permits longitudinal studies of macaques with experimental manipulation and control not possible in human studies (Virdee et al. 2012; Strome and Doudet 2007). Moreover, neuroimaging of the macaque in conjunction with invasive or post mortem studies has been used to elucidate the neural basis of imaging techniques used in humans (Logothetis et al. 2001; Passingham 2009). Many such neuroimaging studies in rhesus macaques would benefit from the convenience and reproducibility of a labelled template image.

The goal of this work was to create a 3D digital brain atlas of the rhesus macaque with labelled ROIs with suitable detail for PET studies. In our approach, we aligned digital images of brain structures delineated in 2D from a widely used rhesus brain atlas (Paxinos et al. 2009) to an MR template image of 112 rhesus subjects (McLaren et al. 2009). We carried out the alignment such that the resulting 3D digital brain atlas consisted of ROIs that can be used to analyze imaging data. As a partial validation, we calculated geometric overlap and compared PET values obtained with the template ROIs against hand-drawn ROIs in striatal and cortical regions. The complete collection of ROIs is available at https://www.nitrc.org/.

Materials and Methods

The 3D digital rhesus brain atlas was created by aligning 2D images to a 3D rhesus MRI template, and it was validated against hand-drawn regions of interest. These steps are detailed below and summarized in Fig. 1.

Two Dimensional Printed Atlas

The three dimensional atlas is based on anatomical information as presented in the two dimensional rhesus atlas, "The Rhesus Monkey Brian in Stereotaxic Coordinates" (Paxinos et al. 2000; Paxinos et al. 2009). This comprehensive atlas is currently the gold standard anatomical reference used by researchers in a wide variety of neurological applications. The Paxinos atlas consists of 151 coronal sections of the brain spaced every 0.45 mm. Nine hundred thirty-six regions were diagrammed and labelled at the hands of leading neuroanatomists based on an extensive review of the literature. Each coronal diagram corresponds to a histologically stained section of tissue from a single subject.

Serial Stacking and 2D Alignment of Digital Tracings

Another group, working in conjunction with the Collations of Connectivity data on the Macaque brain (CoCoMac) project (Stephan et al. 2001; Bakker et al. 2012), constructed digital versions of the print Paxinos figures by tracing all 151 diagrams using graphic design software. The images are rendered

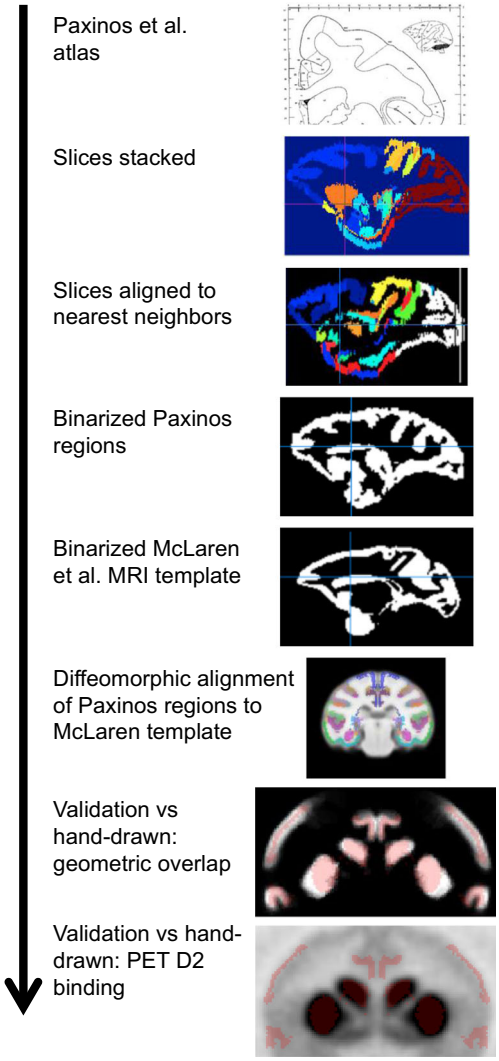

Fig. 1 Summary of steps to create 3D digital rhesus brain atlas

in scalable vector graphics (SVG) format, and a unique RGB color profile was assigned to each of 936 structures, maintaining the nomenclature and abbreviations from the Paxinos atlas (Bezgin et al. 2009). Though not every region in the print atlas is represented, most cortical, striatal, thalamic and amygdaloid structures are included.

After obtaining these coronal SVG images, an intermediate 3D volume was created by stacking them serially anterior to posterior. As the histological slices were each 0.045 mm thick and made at 0.45 mm intervals, the vector images were first converted to TIFF raster images at $(0.45\ \text{mm})^2$ pixel size, such that the pixel edge length was equal to the slice spacing. A nearest neighbor interpolation scheme using minimum Euclidian distance was used, without any anti-aliasing correction in order to preserve both the color index information and fine anatomical detail. Images were then mirrored across central fiducial markers to create symmetric bilateral slices. The RGB color profile information was converted, such that every distinct labelled region was represented by a unique integer. The raster

images were assigned thickness of 0.45 mm. At some points in the extreme rostral and caudal parts of the brain, the frequency of drawings is less than every 0.45 mm, and in these cases, the nearest slice was repeated as necessary to maintain the true relative spacing between the drawn slices. After accounting for the 'missing' slices, there were a total of 168 0.45 mm thick slices that were stacked to make the intermediate volume.

The stacked volume suffered from artifacts introduced in the preparation of the two dimensional slices (Fig. 2). Several types of artifacts, both global and slice specific, commonly result from the brain extraction and slide preparation process (Dauguet 2010). Although the fiducial markers were preserved in the stacking process, the slice-to-slice misregistration is evident in the sagittal view (Fig. 2). Major artifacts observed were the sagging of the dorsal cortex near the center of the brain, and the apparent compression of the temporal lobe towards the caudal end of the brain.

Several techniques have been pursued to correct the slice-specific problems inherent in alignment of a series of 2D histology slices. Both linear and non-linear approaches have been used (Ourselin et al. 2001; MacKenzie-Graham et al. 2004; Ganser et al. 2004; Yushkevich et al. 2006). Due to the presence of the major artifacts in the stacked volume, a three dimensional nonlinear transform method was chosen for the final template registration. However, within the individual two dimensional slices, some minor artifacts were corrected using a simpler linear method.

Within the slices, obvious misalignments were manually corrected using SPAMALIZE software (Oakes n.d.) by translating slices as necessary. Next, an effort was made to align and transform the slices to their neighbors to construct a more cohesive volume. A linear transformation routine was scripted using the FLIRT registration tool allowing 12 degrees of freedom (M Jenkinson and Smith 2001; Mark Jenkinson et al. 2002). Each slice, n, was aligned to the two slices adjacent to it, (n-1) and (n + 1), as well as its neighbors two slices away, (n-2) and (n + 2). The four transformation matrices were weighted and averaged with the adjacent slices each assigned a weight of 3/8 and the distant slices each assigned a weight of 1/8. The weighted transformation matrix was then applied to

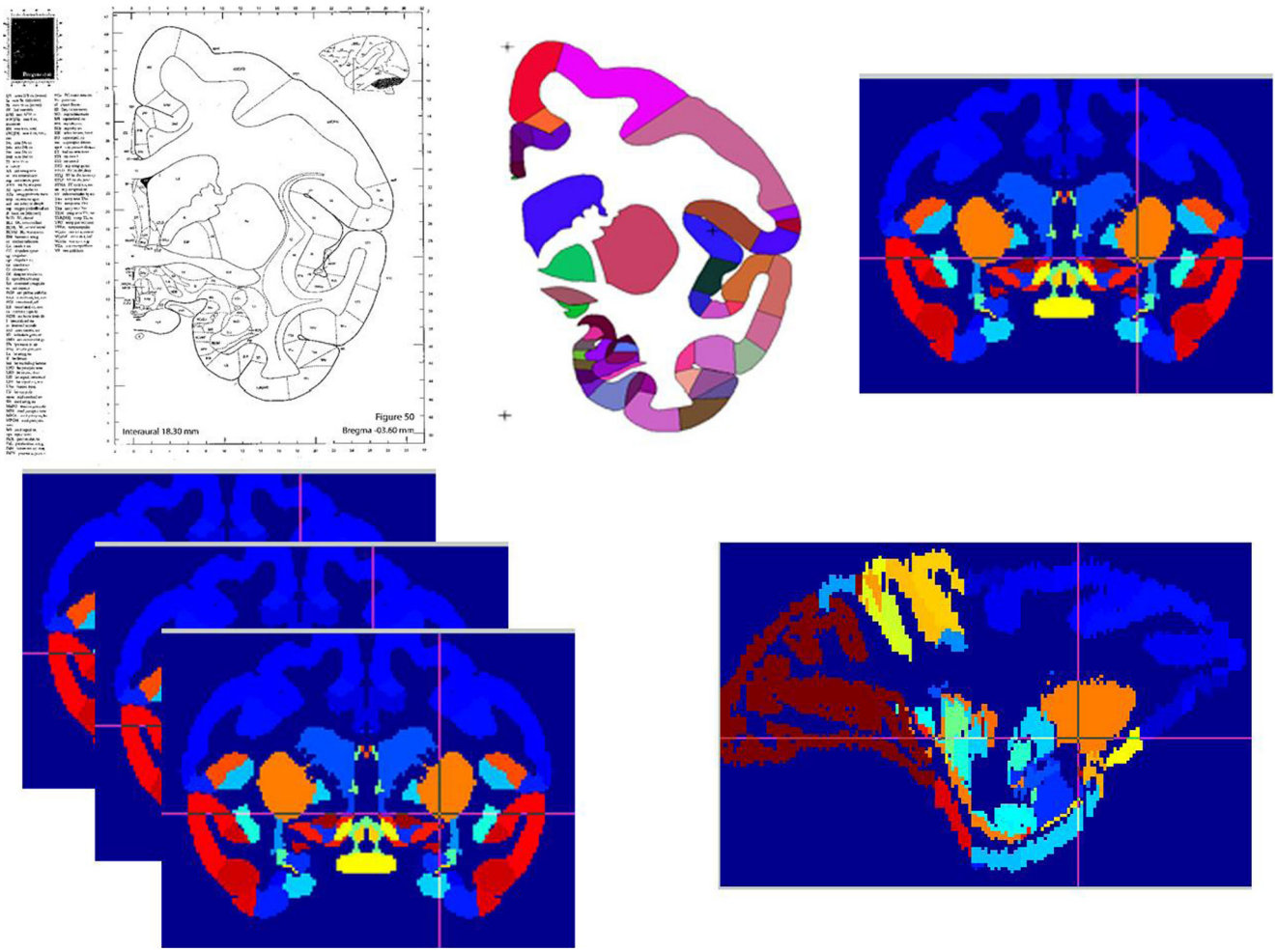

Fig. 2 Initial 3D stacked volume of 2D atlas images. 2D printed atlas (top left), digital version (top mid), mirrored (top right), stacked (bottom left). Note poor alignment in sagittal view (bottom right)

the source slice. The resulting volume (Fig. 3) was a marked improvement from the original stacked volume, but the result was not acceptable as a true representation of the anatomy, as some errors persisted. For example, some sagging of the dorsal cortex near the center of the brain was still apparent (Fig. 3). A major error introduced by this type of alignment is the banana or z-shift effect, in which the natural three dimensional curvatures are lost (Streicher et al. 1997; Malandain et al. 2004). Propagation of error due to individually distorted sections is also a concern (Yushkevich et al. 2006). Even though these and other errors were present, this slice-to-slice alignment step is valuable as it corrects slice-specific deformations and provides a reasonable starting point for the non-linear transformation.

3D Registration to Template

Registration Target

To maximize the utility of the final aligned atlas to the research community, it should be matched to a target template that is presented in a well defined space that is widely accessible, has excellent detail and resolution, and is representative of the subjects being investigated. The template published by McLaren et al. meets these criteria and was used as a target (McLaren et al. 2009). This template contains T1 and T2 weighted population average images of 112 rhesus macaques from three separate sites (mean age 19.7 years). The T1 images were acquired at $0.6 \times 0.6 \times 0.7$ mm^3 ($n = 37$, coronal), $0.47 \times 0.47 \times 1.0$ mm^3 ($n = 15$, coronal), and $0.39 \times 0.39 \times 1.0$ mm^3 ($n = 60$, transaxial). Known as 112RM-SL, this template was constructed iteratively using 12-parameter affine transformations. The 112RM-SL is aligned to the widely referenced D99-SL volume image (Saleem and Logothetis 2006), and thus the atlas presented here will be in a reference space that has been broadly adopted and utilized.

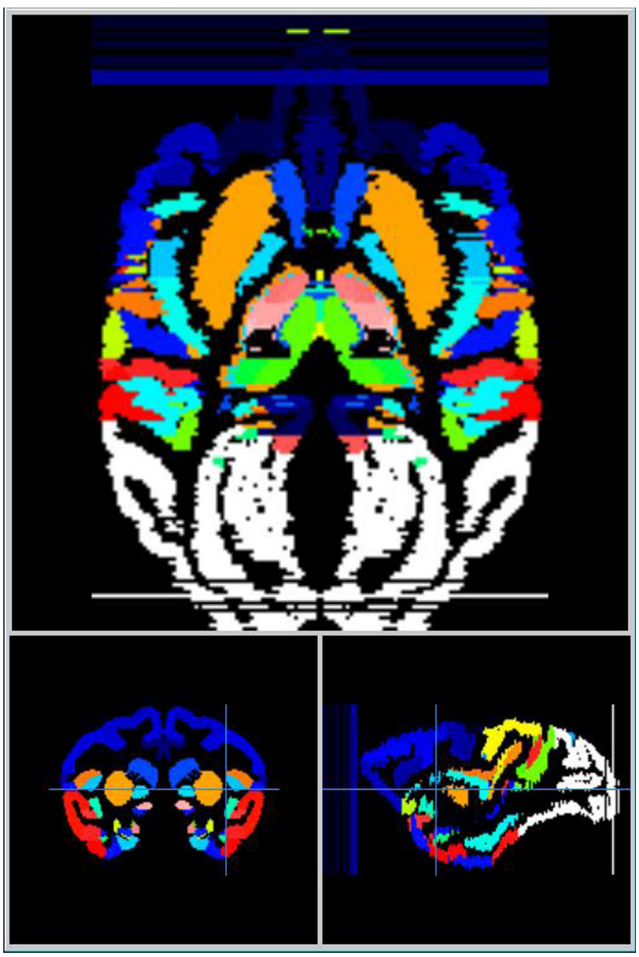

Fig. 3 Intermediate volume. Created by alignment of each coronal slice to 1st and 2nd nearest neighbors in anterior and posterior directions. Not all regions are delineated due to the color scale in this rendition

Because the unilateral Paxinos atlas had been mirrored in a prior step to make a left-right symmetric set of ROIs, the 112RM-SL T1 target template was modified to make it left-right symmetric as well. The volume was rotated approximately one degree about the dorsal-ventral axis to better align the sagittal midplane. A mirror image of the volume was created by flipping each half of the volume across the midplane. The original and mirrored image were then averaged, so that a symmetrical MR image was created to serve as the atlas registration target.

Nonlinear Registration Techniques

To correct the three dimensional global deformations, several different approaches have been used by various groups. Linear approaches have been used with moderate success, but these corrections are global, while local deformations and those between successive slices are not accounted for (Hibbard and Hawkins 1988; Andreasen et al. 1992; Goldszal et al. 1995; Cohen et al. 1998; Malandain et al. 2004; Mega et al. 1997; Yushkevich et al. 2006). Non-linear approaches of both the parametric and non-parametric type have been used to correct the more subtle differences and to allow more flexibility in the transformation routine (Kim et al. 1997; Chakravarty et al. 2006; Chakravarty et al. 2008; Dauguet et al. 2007; Ceritoglu et al. 2010). Though these routines provide visually excellent reconstructions, they are susceptible to stability issues and can introduce errors while processing artifacts such as holes, torn or missing parts and folding common to histological preparations (Dauguet 2010). In this dataset, these types of artifacts were corrected during the drawing process of the Paxinos atlas diagrams, so primarily the three dimensional deformation artifacts remained. Non-linear registration is the best approach to correct for these types of registration issues.

Deformable atlas registrations have been widely used in human brain applications due to the inherent variations in individual brain structure (Thompson et al. 2000). Likewise,

the surface of the rhesus macaque brain contains an intricate pattern of sulci and gyri, so it is reasonable to expect similar issues with variation in structure, both inherent in the anatomy and due to ex-vivo processing.

The nonlinear registration algorithm used here, ANTS (Avants et al. 2008), showed consistent high performance in an evaluation of available nonlinear registration methods (Klein et al. 2009). ANTS uses differentiable deformation fields and normalizes the images by maximizing the cross correlation within the deformation space (Avants et al. 2008). Cross correlation performs well in situations with locally varying intensities, as it depends on the local image average rather than the global approach of other schemes such as mutual information (Studholme et al. 2006). This characteristic makes it well suited for deformable registration.

Final Nonlinear Registration

The 112RM-SL template volume has a voxel size of 0.5 mm × 0.5 mm × 0.5 mm, compared to the intermediate stacked atlas image at 0.45 mm × 0.45 mm × 0.45 mm. The ANTS framework allows for a rigid registration with Euclidian distance nearest neighbor interpolation, so, as an initial step, the atlas volume was aligned and resliced to match the voxel size of the template volume.

Because the atlas image is arbitrarily indexed with integers corresponding to region labels as its intensity information, a direct registration to the in vivo MR template image is impossible. Therefore, a pseudo-MR image was created from the atlas image by setting the indexed values to 1. In this way, the atlas volume became a mask of most of the grey matter in the brain, as white matter and any unlabelled regions had a zero value. The MR template image was segmented into grey matter, white matter and cerebrospinal fluid as detailed below using the FAST segmentation routine (FSL) in order to be an analogue of the pseudo-MR. The white matter and cerebrospinal fluid were zeroed leaving the grey matter. In order to better match the atlas pseudo-MR, grey matter regions that did not appear in the atlas (such as those in the cerebellum) were also zeroed in the segmented grey matter MR template (Fig. 4).

The segmentation of the MR template image presented a number of challenges. As this image would ultimately drive the final transformation, decisions in selecting the segmentation parameters were crucial. In an MR image, the boundary between grey and white matter transitions in a wider gradient than it does anatomically, and not all gray and white matter has the same intensity profile in the MR image. As parameters for the numerical cutoff must be chosen, it was decided to take a conservative approach with respect to the size of the grey matter. Because the atlas regions of interest will ultimately be used to determine functional rather than anatomical data, it is preferable to have the regions of interest lie entirely within the actual anatomical region, rather than have them be too large. Because anatomical and registration variations will come into play when dealing with actual data images, it is prudent to have the atlas regions of interest be slightly smaller and centrally located rather than attempt to extend into areas where the grey matter designation is less than certain.

The main transformation was performed using the grey matter segmented and adjusted 112RM-SL template as the target image, and the slice-aligned stacked atlas grey matter pseudo-MR volume as the source image. The ANTS program was used with its SyN transformation model and cross correlation as the similarity metric. The process was run iteratively on three different sizes of resolution in a multi-level Gaussian pyramid, with a maximum of 100, 100, and 20 runs before convergence at each step size from coarsest to finest resolution. The total deformation was regularized with a Gaussian of 3 pixels in the variance term. The transformations from this step were then applied to the slice-aligned atlas image containing the integer index information to produce the final atlas image aligned in the symmetrized 112RM-SL space. For those wishing to use the ROIs in the 112RM-SL space itself, the symmetrized template was aligned to the original by 6 degrees of freedom and the resulting transformation was applied to the ROIs.

The original hand drawn atlas contained 936 distinct labelled regions. Because many regions were very small and only appeared in a single slice, after the conversion of the 2D vector drawings to 0.5 mm × 0.5 mm × 0.5 mm voxels, 286 regions remained. Several of the smaller regions were combined to provide additional larger composite regions of interest as defined in the literature, e.g. prefrontal cortex. Certain regions that were not included in the original hand drawings were introduced and included as well, such as the cerebellum. These regions were mapped out on the symmetrical target image by hand.

Registration Evaluation

To gauge the accuracy and utility of the atlas image, it was tested using MRI and PET source datasets.

Source Datasets

A set of twenty T1-weighted MR images of adult rhesus macaques with accompanying anatomical regions of interest label sets was used (8 F: 12 M, 6.8 ± 0.8 years, unpublished data). Bilateral caudate and putamen regions had been hand drawn by researchers directly on the T1 MR images using the SPAMALIZE software package. Three bilateral cortical regions were also delineated using fslview: superior temporal gyrus area 2 sulcal and gyral part (ST2), area 6 of the cortex ventral part caudal subdivision (6VC), and anterior cingulate gyrus (ACG). These regions were chosen because they were easily visualized in the MRIs and exhbited significant

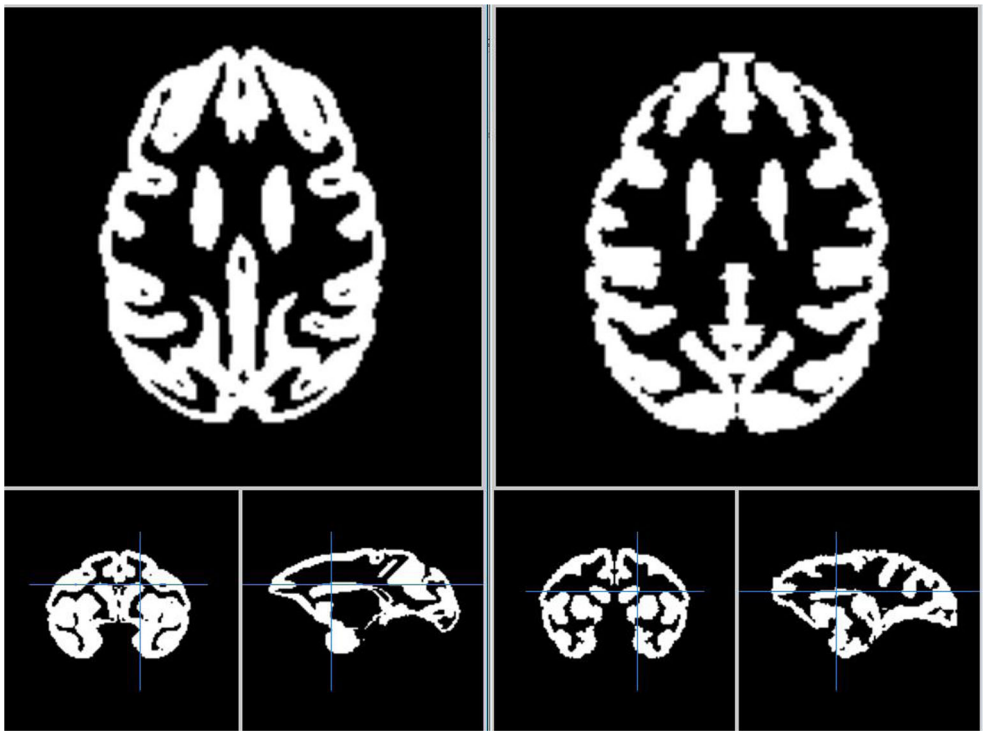

Fig. 4 Pseudo MRIs. MRI T1 template image segmented for grey matter regions of atlas (left) and binarized intermediate atlas image (right)

[^{18}F]fallypride binding in PET. To perform these validations, six delineators drew 477 ROIs consisting of 12,357 slices (Table 1). As this is the typical method in which regions of interest are generated, these hand drawn label sets were assumed to be accurate and treated as the ground truth for the analysis.

The T1 MR images were aligned using FLIRT with a 12 parameter affine transformation to the 112RM-SL T1 image. The transformation matrices from these transforms were applied to the previously drawn striatal region of interest mask images. Following drawing of the cortical ROIs, the MRIs were further aligned using ANTS with deformation field transformations, which were applied to all of the hand drawn ROIs. Thus, all MR images and regions of interest were brought into the same imaging space as the atlas image for direct comparison.

Another dataset was comprised of dynamic PET images of the same subjects acquired using the dopamine D2/D3 receptor antagonist [^{18}F]fallypride. [^{18}F]fallypride accumulates in dopamine receptor rich areas such as the caudate and putamen. Fourteen of the 20 subjects were scanned twice resulting in a total of 34 PET images. These studies were carried out generally following procedures described elsewhere (Converse et al. 2013; Converse et al. 2014). Scans were performed on a microPET P4 under isoflurane anesthesia. Following a Co-57 transmission scan, emission data were acquired for 150 min with [^{18}F]fallypride injected 60 s after scan start (5 mCi i.v.). Events were binned into 5 × 1, 5 × 2, 3 × 5, and 12 × 10 minute frames. Images were reconstructed by filtered backprojection with a ramp filter to 0.95 × 0.95 × 1.21 mm^3 voxels. Early time sum images (0–15 min), which more clearly depict tracer delivery to the whole brain, were aligned to the template iteratively using a 9 parameter affine transformation (flirt). After a preliminary alginment of all images to the 112RM-SL T1 image, the average image was aligned, and the images were aligned within-subject to this aligned average. The resulting transforms were applied to the dynamic images. Images were inspected for motion and corrected as needed. The approximate reconstructed image resolution was 1.7 mm full width at half maximum (FWHM), which remained <2 mm FWHM following the 9 degree of freedom transformation.

Evaluation Metrics

Spatial overlap of the atlas and hand drawn ROIs was evaluated by the mean overlap, also known as the Dice coefficient. The Dice coefficient is the volume of the intersection of the hand drawn (H) and atlas (A) regions divided by their mean volume, $n\{H \cap A\} / ((n\{H\} + n\{A\})/2)$, where $n\{\}$ represents the voxel count in a region (Zijdenbos et al. 1994; Dice 1945). The Dice coefficient ranges from 0 (no overlap) to 1 (perfect overlap).

To evaluate the performance of the atlas when used on a dataset from a study, the binding potential in the regions of interest in the [^{18}F]fallypride PET dataset were calculated using both the hand drawn and atlas generated regions of interest and compared for similarity. Binding potentials were

Table 1 Validation of atlas ROIs

Region	ST2		6VC		ACG		Cd[a]		Pu		Mean[b]
n drawers	4		4		2		1		1		
	Left	Right	Left	Right	Left	Right	Left	Right	Left	Right	
n hand ROIs[c]	79	79	79	80	40	40	20	20	20	20	
Volume (uL)											
Atlas	113	113	128	128	532	532	534	535	713	713	404 ± 254
Hand[d]	119 ± 11	119 ± 12	321 ± 48	318 ± 40	567 ± 185	583 ± 180	485	494	732	748	449 ± 225
Overlap (Dice)											
Atlas vs hand[e]	0.46 ± 0.02	0.51 ± 0.01	0.38 ± 0.04	0.39 ± 0.03	0.68 ± 0.02	0.69 ± 0.02	0.74	0.74	0.73	0.73	0.61 ± 0.15
Inter-rater[f]	0.72 ± 0.05	0.73 ± 0.06	0.71 ± 0.10	0.72 ± 0.11	0.65	0.66	–	–	–	–	0.70 ± 0.03
[^{18}F]fallypride binding BP_{ND}											
Atlas[g]	1.21 ± 0.14	1.44 ± 0.14	1.19 ± 0.29	1.16 ± 0.19	1.41 ± 0.12	1.40 ± 0.11	20.1 ± 2.9	20.4 ± 2.7	24.0 ± 3.2	23.2 ± 3.0	9.5 ± 10.7
Hand[h]	1.19 ± 0.02	1.38 ± 0.01	1.22 ± 0.01	1.13 ± 0.02	1.40 ± 0.01	1.37 ± 0.02	21.5	21.8	23.5	22.8	9.7 ± 10.9
Pearson r											
Atlas vs hand[i]	0.85 ± 0.04	0.89 ± 0.02	0.94 ± 0.01	0.91 ± 0.02	0.98 ± 0.01	0.94 ± 0.03	0.93	0.90	0.96	0.95	0.92 ± 0.04
Inter-rater[j]	0.92 ± 0.06	0.87 ± 0.06	0.93 ± 0.07	0.97 ± 0.02	0.98	0.97	–	–	–	–	0.94 ± 0.04

More detailed results are presented in Supplementary Table I

[a] The caudate ROI here includes only head and body as the tail was not delineated by hand. Also, in this analysis, 8 voxels were accidentally erased from the left caudate, but this 0.2% reduction in volume is not expected to have substantially altered any results

[b] Mean and SD of these means over ROIs

[c] Each drawer drew ROIs on each of the 20 subjects' MRIs except for one drawer, who missed 3 regions, hence $n = 79$ for those ROIs

[d] For each drawer, mean volume was calculated over all subjects' MRIs (n = 20). Mean and SD over those means is reported

[e] For each drawer, mean Dice coefficient vs atlas was calculated over all subjects' MRIs. Mean and SD over those means is reported

[f] For each possible combination of drawers, mean Dice coefficient was calculated over all subjects. Mean and SD over those means is reported

[g] Mean and SD ($n = 34$) over all subjects' PET scans of BP_{ND} calculated using atlas ROI

[h] For each drawer, mean of BP_{ND} was calculated over all subjects' PET scans. Mean and SD over those means is reported

[i] For each drawer, the correlation of BP_{ND} vs atlas value was calculated over all subjects' PET scans. Mean and SD over those r values is reported

[j] For each possible combination of drawers, the correlation of BP_{ND} values was calculated over all subjects. Mean and SD over those r values is reported

calculated using the Logan graphical analysis method with a cerebellar reference region (Logan et al. 1996). The reference region is a cerebellar gray matter area drawn to exclude vermis and avoid spillover from adjoining regions (see Supplemental Fig. 1). Binding potentials for the atlas ROIs were compared to hand drawn by linear regression.

Results

Qualitative Evaluation

Visually, the non-linear registration of the atlas to the MR template appears favorable. Major global artifacts that were present in the stacked volume were addressed, such as the sagging dorsal cortex and the compressed temporal lobe. The dimensions of the atlas closely matched the template, and most major sulci and gyri appeared to fall in the correct arrangement. Fig. 5 shows the atlas volume overlaid on the template MR image to demonstrate the overall agreement between the two volumes. Atlas ROIs are compared to hand drawn ROIs and shown on a PET [^{18}F]fallypride image in Fig. 6.

Quantitative Evaluation

A subset of atlas ROIs were quantitatively validated against hand drawn ROIs by calculating their spatial overlaps and comparing PET binding potentials (Table 1). The atlas volumes agreed with the hand drawn volumes to better than 10%, except for 6VC, for which the atlas volume was only 40% of the hand drawn. The Dice coefficients were 61 ± 15% (mean

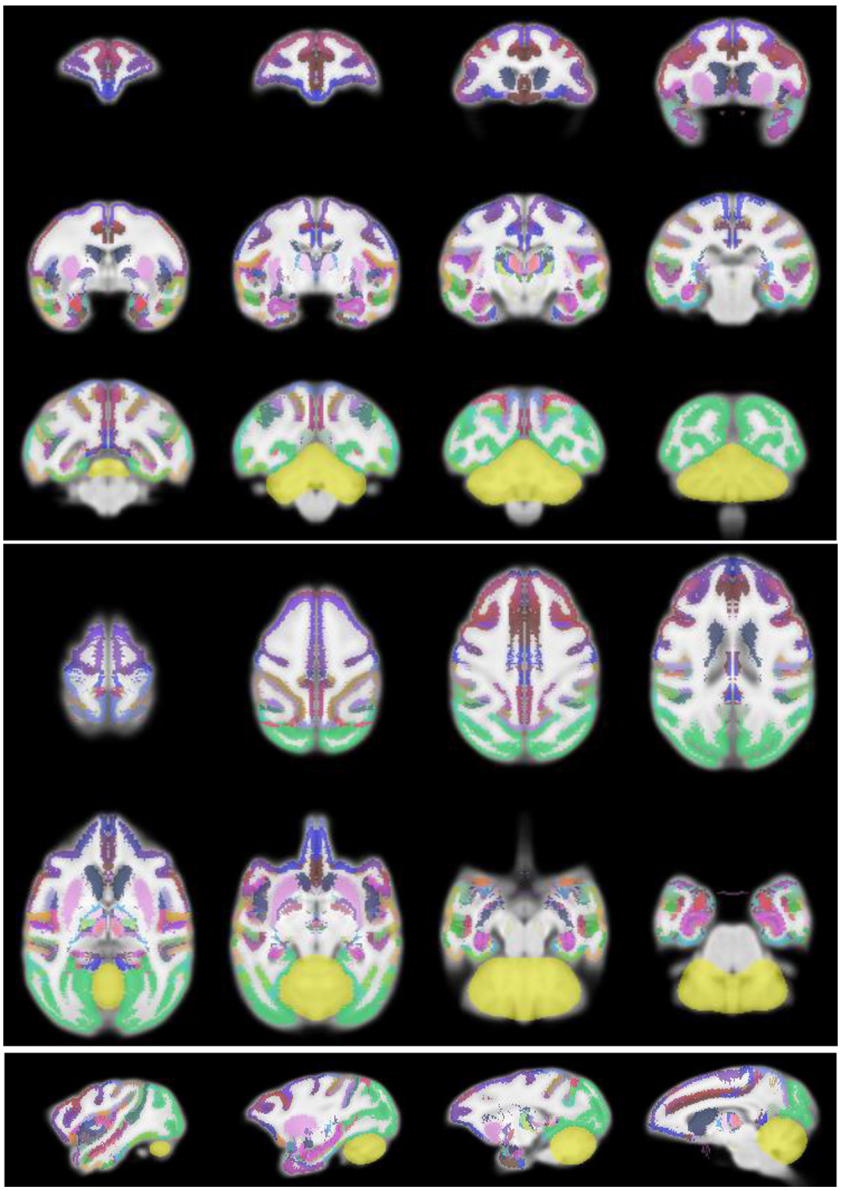

Fig. 5 Final alignment. Atlas ROIs overlaid on MRI template. Every tenth 0.5 mm slice shown. Coronal (top), axial (mid), and sagittal (bottom)

± s.d. over 10 regions, range 38% - 74%). For 6VC, the overlap was relatively poor apparently because the hand drawn regions were large, and the overlap for ST2 appeared to suffer because the template region did not extend as far laterally as the hand drawn. When comparing regions of unequal volumes, the maximum possible Dice coefficient, which occurs when the smaller region is entirely contained within the larger region, is less than one. The Dice coefficients divided by their maximum possible values ranged from 51 to 80% over the ten regions (Supplementary Table 1).

Binding potentials for [^{18}F]fallypride are shown as well in Table 1 and also in Fig. 7. There was good agreement between binding calculated using atlas and hand drawn regions ($r = 0.92 \pm 0.04$, range 0.85–0.98). The variance in binding over the 34 scans of 20 subjects using the hand drawn ROIs was comparable to that using the template ROIs (Supplementary Table 1). In regions for which multiple drawers delineated ROIs, correlations over subjects of atlas vs. hand based binding were generally comparable to inter-rater correlations (Table 1).

Discussion

We have described here the creation of an anatomically labelled rhesus macaque brain imaging template. This work was driven by the desire to conveniently and reproducibly analyze PET imaging data using established ROIs. This result demonstrates the successful application of a general procedure for aligning a 2D labelled atlas to a 3D imaging template with good accuracy while maintaining contiguity of individual ROIs.

We expect this labelled template will be generally useful for rhesus macaque neuroimaging analysis. As we showed by validating against hand drawn ROIs, the labelled template is suitable for analysis of PET data in cortical and subcortical regions, but we note two caveats. First, the animals used in the MR template were older than those used in typical imaging studies. Second, because the Paxinos regions are unilateral, we applied them to a symmetrized version of the MRI template. The literature suggests that macaque brain anatomy is relatively symmetric compared to humans and chimpanzees (Heilbroner and Holloway 1989; Bogart et al. 2012; Hopkins et al. 2015), nevertheless we also provide a set of regions aligned to the original MRI template. We also note that, despite the registration to a relatively coarse 0.5 mm cubic voxel space, the fine anatomical detail of the original Paxinos drawings still appears in this version. In some applications, it might be beneficial to smooth the regions to better match the scanner image resolution. Additionally, we note that in creating the binary target image, it might have been more accurate to perform a manual, rather than the automated, segmentation.

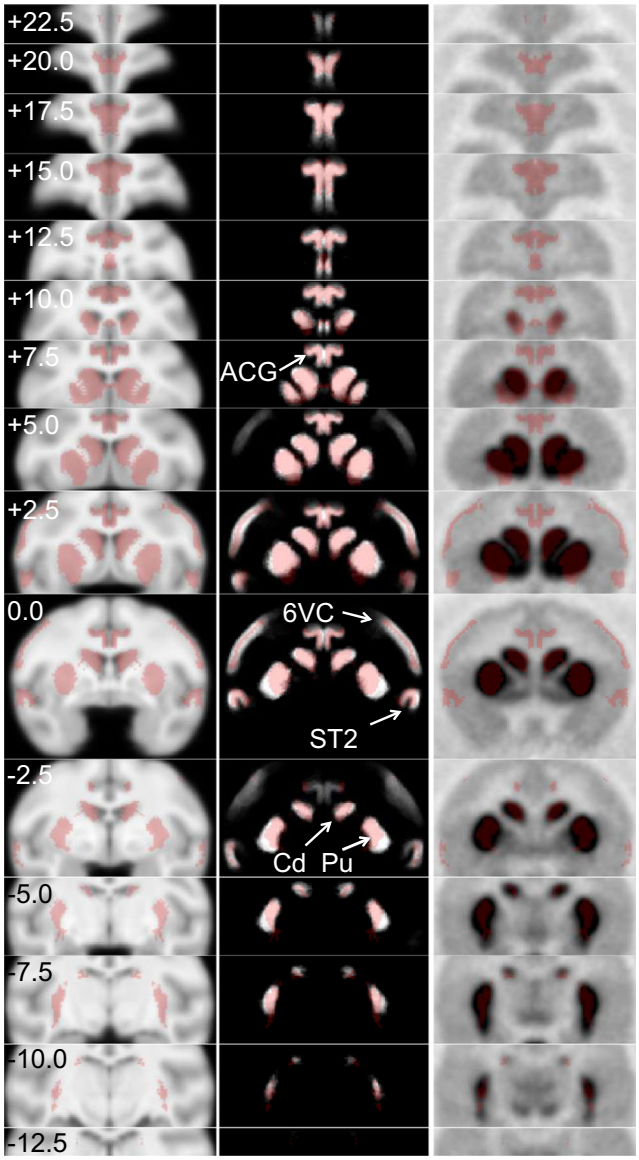

Fig. 6 Qualitative validation of alignment. Selected atlas ROIs (red) overlaid on (left) template MRI, (center) average over all delineators and all subjects of hand drawn ROIs, and (right) average fallypride radioactivity image (0–19 min post-injection, individual images scaled to injected dose / body weight). Coronal slices are shown from 22.5 mm anterior (top row) to12.5 mm posterior (bottom row) relative to anterior commissure. ACG = anterior cingulate gyrus, 6VC = area 6 of the cortex ventral part caudal subdivision, ST2 = superior temporal sulcus area 2, Cd = caudate nucleus, Pu = putamen. See Table 1 for further details

Other labelled macaque templates have been reported in the literature (Frey et al. 2011; Rohlfing et al. 2012; Van Essen et al. 2012; Reveley et al. 2017; Shi et al. 2017). The present work is distinguished from these in that (1) the parcellation is based upon the widely used Paxinos et al. (2009) atlas, (2) the target 3D template is based on over 100 rhesus MRIs (McLaren et al. 2009), (3) the resulting labelled regions are easily extracted and therefore appropriate for ROI analysis, and (4) it has been partially validated against hand drawn ROIs.

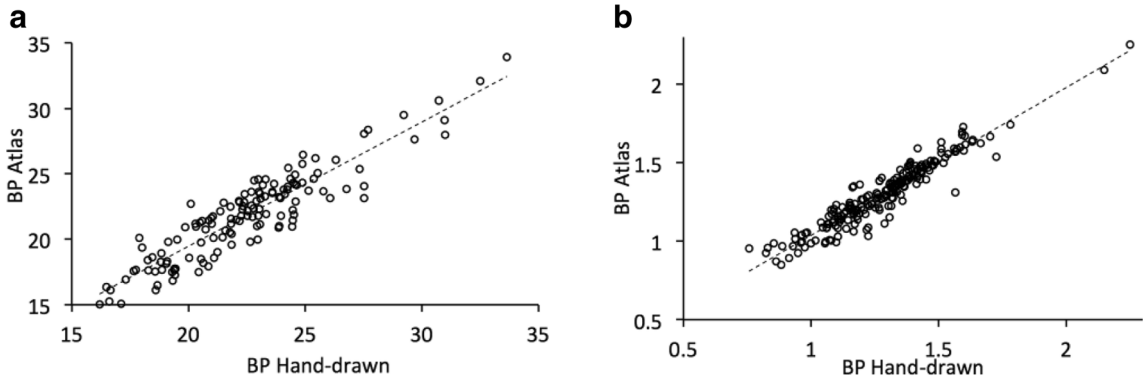

Fig. 7 Validation by [^{18}F]fallypride binding potential comparison. Regional binding potentials calculated using atlas vs. hand drawn ROIs. **a** Striatal regions: caudate (head and body combined) and putamen. Best fit shown y = 0.95 x + 0.40, $r = 0.92$, $n = 136$, $p < 10^{-5}$. **b** Cortical regions: ACG, 6VC, and ST2. y = 0.94 x + 0.09, $r = 0.97$, $n = 204$, $p < 10^{-5}$. Comparisons of left and right ROIs over 34 scans of 20 subjects. For cortical regions, hand-drawn BP is mean over multiple delineators. See Table 1 for further details

We expect these anatomically defined regions may be useful to other researchers. They are appropriate for analysis of PET data, particularly of striatal and cortical binding of dopaminergic tracers (Converse et al. 2013; Converse et al. 2014). Among other applications of interest may be the definition of seed and target ROIs for connectivity analyses (Adluru et al. 2012; Zakszewski et al. 2014).

Conclusions

Motivated by the need to conveniently and reproducibly perform ROI analyses of PET data, we have aligned a widely used 2D rhesus macaque atlas to a published rhesus macaque MRI template. A subset of striatal and cortical regions have been validated for analysis of PET data. ROIs from this labeled template have been used now in a number of studies (Converse et al. 2013; Converse et al. 2014; Christian et al. 2013; Wooten et al. 2013; Hillmer et al. 2014; Adluru et al. 2012; Zakszewski et al. 2014), and we make them available here to the wider neuroimaging community.

Information Sharing Statement

The labeled template described here is freely available at the Neuroimaging Informatics Tools and Resources Clearinghouse (NITRC) at https://www.nitrc.org/.

Acknowledgements This work was primarily funded by NIH grant R21EB004482 to A.K.C. with additional support from R01AA012277, P50MH100031, and U54HD090256. G.Y.B. acknowledges JS McDonnell Collaborative Research Grant 220020255. The authors are grateful to Mary L. Schneider for the use of PET and MR images. The authors are grateful to Max Albiero, Erin Crain, Shilpa Cyriac, Sabrina Koehler, Parker Johnson, and Alysha Rameshk for assistance drawing and analyzing ROIs for validation.

References

Adluru, N., Zhang, H., Fox, A. S., Shelton, S. E., Ennis, C. M., Bartosic, A. M., Oler, J. A., et al. (2012). A diffusion tensor brain template for rhesus macaques. *NeuroImage, 59*(1), 306–318.

Andreasen, A., Drewes, A. M., Assentoft, J. E., & Larsen, N. E. (1992). Computer-assisted alignment of standard serial sections without use of artificial landmarks. A practical approach to the utilization of incomplete information in 3-D reconstruction of the hippocampal region. *Journal of Neuroscience Methods, 45*(3), 199–207.

Avants, B. B., Epstein, C. L., Grossman, M., & Gee, J. C. (2008). Symmetric diffeomorphic image registration with cross-correlation: evaluating automated labeling of elderly and neurodegenerative brain. *Medical Image Analysis, 12*(1), 26–41.

Bakker, R., Wachtler, T., & Diesmann, M. (2012). CoCoMac 2.0 and the future of tract-tracing databases. *Frontiers in Neuroinformatics, 6*, 30. https://doi.org/10.3389/fninf.2012.00030.

Ballanger, B., Tremblay, L., Sgambato-Faure, V., Beaudoin-Gobert, M., Lavenne, F., Le Bars, D., & Costes, N. (2013). A multi-atlas based method for automated anatomical Macaca Fascicularis brain MRI segmentation and PET kinetic extraction. *NeuroImage, 77*, 26–43. https://doi.org/10.1016/j.neuroimage.2013.03.029.

Bezgin, G., Reid, A. T., Schubert, D., & Kötter, R. (2009). Matching spatial with ontological brain regions using Java tools for visualization, database access, and integrated data analysis. *Neuroinformatics, 7*(1), 7–22.

Bogart, S. L., Mangin, J.-F., Schapiro, S. J., Reamer, L., Bennett, A. J., Pierre, P. J., & Hopkins, W. D. (2012). Cortical sulci asymmetries in chimpanzees and macaques: a new look at an old idea. *NeuroImage, 61*(3), 533–541. https://doi.org/10.1016/j.neuroimage.2012.03.082.

Ceritoglu, C., Wang, L., Selemon, L. D., Csernansky, J. G., Miller, M. I., & Tilak Ratnanather, J. (2010). Large deformation diffeomorphic metric mapping registration of reconstructed 3D histological section images and in vivo MR images. *Frontiers in Human Neuroscience, 4*, 43.

Chakravarty, Mallar, M., Bertrand, G., Hodge, C. P., Sadikot, A. F., & Louis Collins, D. (2006). The creation of a brain atlas for image guided neurosurgery using serial histological data. *NeuroImage, 30*(2), 359–376.

Chakravarty, Mallar, M., Frey, S., Collins, D. L. (2008). Digital atlas of the Rhesus Monkey brain in stereotaxic coordinates. In *The rhesus monkey brain in stereotaxic coordinates*, 2nd ed. Elsevier.

Christian, B. T., Wooten, D. W., Hillmer, A. T., Tudorascu, D. L., Converse, A. K., Moore, C. F., Ahlers, E. O., et al. (2013). Serotonin transporter genotype affects serotonin 5-HT1A binding

in primates. *The Journal of Neuroscience, 33*(6), 2512–2516. https://doi.org/10.1523/JNEUROSCI.4182-12.2013.

Cohen, F. S., Yang, Z., Huang, Z., & Nissanov, J. (1998). Automatic matching of homologous histological sections. *IEEE Transactions on Biomedical Engineering, 45*(5), 642–649.

Converse, A. K., Moore, C. F., Moirano, J. M., Ahlers, E. O., Larson, J. A., Engle, J. W., Barnhart, T. E., et al. (2013). Prenatal stress induces increased striatal dopamine transporter binding in adult nonhuman Primates. *Biological Psychiatry, 74*(7), 502–510. https://doi.org/10.1016/j.biopsych.2013.04.023.

Converse, A. K., Moore, C. F., Holden, J. E., Ahlers, E. O., Moirano, J. M., Larson, J. A., Resch, L. M., et al. (2014). Moderate-level prenatal alcohol exposure induces sex differences in dopamine D1 receptor binding in adult rhesus monkeys. *Alcoholism, Clinical and Experimental Research, 38*(12), 2934–2943. https://doi.org/10.1111/acer.12575.

Dauguet, J. (2010). Three-dimensional histological imaging of primate brain and correlation with in vivo medical device images. *Revue de Primatologie*, February. Société francophone de primatologie. https://doi.org/10.4000/primatologie.546.

Dauguet, J., Delzescaux, T., Condé, F., Mangin, J.-F., Ayache, N., Hantraye, P., & Frouin, V. (2007). Three-dimensional reconstruction of stained histological slices and 3D non-linear registration with in-vivo MRI for whole baboon brain. *Journal of Neuroscience Methods, 164*(1), 191–204.

Dice, L. R. (1945). Measures of the amount of ecologic association between species. *Ecology, 26*(3), 297–302.

Essen, V., David, C., Glasser, M. F., Dierker, D. L., & Harwell, J. (2012). Cortical Parcellations of the macaque monkey analyzed on surface-based atlases. *Cerebral Cortex, 22*(10), 2227–2240. https://doi.org/10.1093/cercor/bhr290.

Frey, S., Pandya, D. N., Mallar Chakravarty, M., Bailey, L., Petrides, M., & Louis Collins, D. (2011). An MRI based average macaque monkey stereotaxic atlas and space (MNI monkey space). *NeuroImage, 55*(4). ACADEMIC PRESS INC ELSEVIER SCIENCE), 1435–1442. https://doi.org/10.1016/j.neuroimage.2011.01.040.

Ganser, K. A., Dickhaus, H., Metzner, R., & Wirtz, C. R. (2004). A deformable digital brain atlas system according to Talairach and Tournoux. *Medical Image Analysis, 8*(1), 3–22.

Goldszal, A. F., Tretiak, O. J., Hand, P. J., Bhasin, S., & McEachron, D. L. (1995). Three-dimensional reconstruction of activated columns from 2-[14C]deoxy-D-glucose data. *NeuroImage, 2*(1), 9–20.

Heilbroner, P. L., & Holloway, R. L. (1989). Anatomical brain asymmetry in monkeys: frontal, temporoparietal, and limbic cortex in Macaca. *American Journal of Physical Anthropology, 80*(2), 203–211. https://doi.org/10.1002/ajpa.1330800208.

Hibbard, L. S., & Hawkins, R. A. (1988). Objective image alignment for three-dimensional reconstruction of digital autoradiograms. *Journal of Neuroscience Methods, 26*(1), 55–74.

Hillmer, A. T., Wooten, D. W., Tudorascu, D. L., Barnhart, T. E., Ahlers, E. O., Resch, L. M., Larson, J. A., et al. (2014). The effects of chronic alcohol self-administration on serotonin-1A receptor binding in nonhuman Primates. *Drug and Alcohol Dependence, 144*, 119–126. https://doi.org/10.1016/j.drugalcdep.2014.08.015.

Hopkins, W.D., Misiura, M., Pope, S.M., & Latash, E. M. (2015). Behavioral and brain asymmetries in primates: A preliminary evaluation of two evolutionary hypotheses." In Miller, MB, Kingstone, A (eds.) *Year in Cognitive Neuroscience* 1359:65–83. Annals of the New York Academy of Sciences. https://doi.org/10.1111/nyas.12936.

Jenkinson, M., & Smith, S. (2001). A global optimisation method for robust affine registration of brain images. *Medical Image Analysis, 5*(2), 143–156.

Jenkinson, M., Bannister, P., Brady, M., & Smith, S. (2002). Improved optimization for the robust and accurate linear registration and motion correction of brain images. *NeuroImage, 17*(2), 825–841.

Kim, B., Boes, J. L., Frey, K. A., & Meyer, C. R. (1997). Mutual information for automated unwarping of rat brain autoradiographs. *NeuroImage, 5*(1), 31–40.

Klein, A., Andersson, J., Ardekani, B. A., Ashburner, J., Avants, B., Chiang, M.-C., Christensen, G. E., et al. (2009). Evaluation of 14 nonlinear deformation algorithms applied to human brain MRI registration. *NeuroImage, 46*(3), 786–802.

Logan, J., Fowler, J. S., Volkow, N. D., Wang, G. J., Ding, Y. S., & Alexoff, D. L. (1996). Distribution volume ratios without blood sampling from graphical analysis of PET data. *Journal of Cerebral Blood Flow and Metabolism, 16*(5), 834–840.

Logothetis, N. K., Pauls, J., Augath, M., Trinath, T., & Oeltermann, A. (2001). Neurophysiological investigation of the basis of the FMRI signal. *Nature, 412*(6843), 150–157.

MacKenzie-Graham, A., Lee, E.-F., Dinov, I. D., Bota, M., Shattuck, D. W., Ruffins, S., Yuan, H., et al. (2004). A multimodal, multidimensional atlas of the C57BL/6J mouse brain. *Journal of Anatomy, 204*(2), 93–102.

Malandain, G., Bardinet, E., Nelissen, K., & Vanduffel, W. (2004). Fusion of autoradiographs with an MR volume using 2-D and 3-D linear transformations. *NeuroImage, 23*(1), 111–127.

McLaren, D. G., Kosmatka, K. J., Oakes, T. R., Kroenke, C. D., Kohama, S. G., Matochik, J. a., Ingram, D. K., & Johnson, S. C. (2009). A population-average MRI-based atlas collection of the rhesus macaque. *NeuroImage, 45*(1), 52–59. https://doi.org/10.1016/j.neuroimage.2008.10.058.

Mega, M. S., Chen, S. S., Thompson, P. M., Woods, R. P., Karaca, T. J., Tiwari, A., Vinters, H. V., Small, G. W., & Toga, A. W. (1997). Mapping histology to metabolism: Coregistration of stained whole-brain sections to Premortem PET in alzheimer's disease. *NeuroImage, 5*(2), 147–153.

Oakes, T R. (n.d.) Spamalize: http://Brainimaging.Waisman.Wisc.Edu/~oakes/Spam/Spam_frames.Htm.

Ourselin, S, A Roche, G Subsol, X Pennec, and N Ayache. 2001. "Reconstructing a 3D structure from serial histological sections." Image and Vision Computing 19 (1–2, SI): 25–31. doi:https://doi.org/10.1016/S0262-8856(00)00052-4.

Passingham, R. (2009). How good is the macaque monkey model of the human brain? *Current Opinion in Neurobiology, 19*(1), 6–11. https://doi.org/10.1016/j.conb.2009.01.002.

Paxinos, G., Huang, X.-F., & Toga, A. W. (2000). *The rhesus monkey brain in stereotaxic coordinates*. Cambridge: Academic Press.

Paxinos, G., Huang, X.-F., Petrides, M., & Toga, A. W. (2009). *The rhesus monkey brain in stereotaxic coordinates* (2nd ed.). Cambridge: Academic Press.

Reveley, C., Gruslys, A., Ye, F. Q., Glen, D., Samaha, J., Russ, B. E., Saad, Z., Seth, A. K., Leopold, D. A., & Saleem, K. S. (2017). Three-dimensional digital template atlas of the macaque brain. *Cerebral Cortex, 27*(9), 4463–4477. https://doi.org/10.1093/cercor/bhw248.

Rohlfing, T., Kroenke, C. D., Sullivan, E.V., Dubach, M. F., Bowden, D. M, Grant, K. A., & Pfefferbaum, A.. (2012). The INIA19 template and NeuroMaps atlas for primate brain image parcellation and spatial normalization. Front Neuroinform 6. https://doi.org/10.3389/fninf.2012.00027.

Rubins, D. J., Melega, W. P., Lacan, G., Way, B., Plenevaux, A., Luxen, A., & Cherry, S. R. (2003). Development and evaluation of an automated atlas-based image analysis method for MicroPET studies of the rat brain. *NeuroImage, 20*(4), 2100–2118.

Saleem, K. S., & Logothetis, N. K. (2006). *A combined MRI and histology atlas of the rhesus monkey brain*. Amsterdam: Academic Press.

Shi, Y., Budin, F., Yapuncich, E., Rumple, A., Young, J. T, Payne, C., Zhang, X, et al. (2017). UNC-emory infant atlases for macaque brain image analysis: postnatal brain development through 12 months. Front Neurosci 10. https://doi.org/10.3389/fnins.2016.00617.

Stephan, K. E., Kamper, L., Bozkurt, A., Burns, G. A., Young, M. P., & Kötter, R. (2001). Advanced database methodology for the collation of connectivity data on the macaque brain (CoCoMac). *Philosophical Transactions of the Royal Society of London. Series B, Biological Sciences, 356*(1412), 1159–1186.

Stephan, K. E., McIntosh, A. R., Hilgetag, C. C. (2010). In Memoriam: Rolf Kötter (1961–2010). *PLoS Computational Biology, 6*(10), e1000965. https://doi.org/10.1371/journal.pcbi.1000965.

Streicher, J., Weninger, W. J., & Müller, G. B. (1997). External marker-based automatic Congruencing: a new method of 3D reconstruction from serial sections. *The Anatomical Record, 248*(4), 583–602.

Strome, E. M., & Doudet, D. J. (2007). Animal models of neurodegenerative disease: Insights from in vivo imaging studies. *Molecular Imaging and Biology, 9*(4), 186–195. https://doi.org/10.1007/s11307-007-0093-4.

Studholme, C., Drapaca, C., Iordanova, B., & Cardenas, V. (2006). Deformation-based mapping of volume change from serial brain MRI in the presence of local tissue contrast change. *IEEE Transactions on Medical Imaging, 25*(5), 626–639.

Tai, Y. C., Chatziioannou, A., Siegel, S., Young, J., Newport, D., Goble, R. N., Nutt, R. E., & Cherry, S. R. (2001). Performance evaluation of the MicroPET P4: A PET system dedicated to animal imaging. *Physics in Medicine and Biology, 46*(7), 1845–1862.

Thompson, P. M., Woods, R. P., Mega, M. S., & Toga, A. W. (2000). Mathematical/computational challenges in creating deformable and probabilistic atlases of the human brain. *Human Brain Mapping, 9*(2), 81–92.

Tzourio-Mazoyer, N., Landeau, B., Papathanassiou, D., Crivello, F., Etard, O., Delcroix, N., Mazoyer, B., & Joliot, M. (2002). Automated anatomical labeling of activations in SPM using a macroscopic anatomical Parcellation of the MNI MRI single-subject brain. *NeuroImage, 15*(1), 273–289. https://doi.org/10.1006/nimg.2001.0978.

Virdee, K., Cumming, P., Caprioli, D., Jupp, B., Rominger, A., Aigbirhio, F. I., Fryer, T. D., Riss, P. J., & Dalley, J. W. (2012). Applications of positron emission tomography in animal models of neurological and neuropsychiatric disorders. *Neuroscience and Biobehavioral Reviews, 36*(4), 1188–1216. https://doi.org/10.1016/j.neubiorev.2012.01.009.

Wooten, D. W., Hillmer, A. T., Moirano, J. M., Tudorascu, D. L., Ahlers, E. O., Slesarev, M. S., Barnhart, T. E., Mukherjee, J., Schneider, M. L., & Christian, B. T. (2013). 5-HT1A sex based differences in Bmax, in vivo KD, and BPND in the nonhuman primate. *NeuroImage, 77*, 125–132. https://doi.org/10.1016/j.neuroimage.2013.03.027.

Yushkevich, P. A., Avants, B. B., Ng, L., Hawrylycz, M., Burstein, P. D., Zhang, H., & Gee, J. C. (2006). 3D Mouse brain reconstruction from histology using a coarse-to-fine approach. In Pluim, J. P. W., Likar, B., & Gerritsen, F. A. (eds) *Biomedical Image Registration, Proceedings*, 4057:230–37. Lecture Notes in Computer Science.

Zakszewski, E., Adluru, N., Tromp, D. P. M., Kalin, N., & Alexander, A. L. (2014). A diffusion-tensor-based white matter atlas for rhesus macaques. *PLoS One, 9*(9). https://doi.org/10.1371/journal.pone.0107398.

Zijdenbos, A. P., Dawant, B. M., Margolin, R. A., & Palmer, A. C. (1994). Morphometric analysis of white matter lesions in MR images: Method and validation. *IEEE Transactions on Medical Imaging, 13*(4), 716–724.